Published: Zhiyuan Shen, Shuting Chen, Lei Zhang, Kui Yao, and Chin Yaw Tan, "Direct-Write Piezoelectric Ultrasonic Transducers for Non-Destructive Testing of Metal Plates," IEEE Sensors Journal, Vol. 17, No. 11, pp. 3354-3361, 2017. (10.1109/JSEN.2017.2694454)

Direct-Write Piezoelectric Ultrasonic Transducers for Non-Destructive Testing of Metal Plates

Zhiyuan Shen, *Member, IEEE*, Shuting Chen, Lei Zhang, *Member, IEEE*, Kui Yao[1], *Senior Member, IEEE*, and Chin Yaw Tan, *Member, IEEE*

***Abstract*—Current real time structural health monitoring is implemented by assembling multiple discrete sensors on a structure with each sensor providing only point measurement. The installation of the multiple sensors results in high global cost and low reliability. This paper reports the design, direct-write fabrication, and testing of ultrasonic transducers on a plate structure and a non-destructive testing method for detecting defects using the sensor array comprising the direct-write ultrasonic transducers. The transducers are made of piezoelectric poly(vinylidenefluoride/trifluoroethylene) (P(VDF/TrFE)) polymer coatings that are aerosol-spray deposited and patterned directly on the plate structure to be monitored. The ultrasonic transducers bearing annular array comb electrodes are designed for generating and selectively detecting fundamental antisymmetric Lamb mode ultrasonic waves in the plate structure. The ultrasonic transducers can serve as both the actuators to generate ultrasonic waves and the sensors to detect ultrasonic waves. The ultrasonic waves propagating through the plate structure contain the information about the structural integrity. With copper bars of different thicknesses introduced at the plate centre as mock defects of different severity, the correlation between the transducer response and the defect thickness and hence the severity is verified. It is also demonstrated that four ultrasonic transducers located at the square plate (100 mm×100 mm×1.27 mm) corners forming a transducer array which can locate the defect on the plate. A short time Fourier transform algorithm and an imaging algorithm are developed for processing signal of the pitch-catch ultrasonic wave spectra to determine the location of the defects, which is verified by experimental results.**

***Index Terms*—Direct-write, Non-destructive testing, Piezoelectric polymer, Sensor, Ultrasonic transducers**

I. Introduction

THE AVIATION INDUSTRY has been increasingly demanding for non-destructive testing (NDT) methods with real-time structural health monitoring capability [1]. Distributed sensor-networks are a promising technology to fulfill this requirement. Existing sensor-networks are mainly realized by installing multiple discrete sensors on the aeronautical parts under monitoring [2]. The weight and profile of the sensors, cabling connections and associated equipment, however, pose a significant problem for aircrafts which are very sensitive to weight increment. Direct-write (DW) sensor network on the aeronautical part is a promising approach to integrate the sensor assembling process with the aeronautical manufacturing process, for achieving reduced total cost and improved system reliability [3].

Direct-write refers to a group of processes which can precisely deposit functional and/or structural materials on some structural parts. These materials are processed *in situ* on the structure, and are directly patterned to the shape used in the final components [4]. As an additive on-demand manufacture process, direct-write approach is able to deposit various materials and has the advantage of being able to realize conformal large area deposition [5]. The line width of the deposited pattern can have the feature size of micrometers and the deposited layer thickness can vary from tens of nanometers to hundreds of micrometers [6]-[9]. Based on the mechanisms of material handling and transfer, the direct-write technologies can be categorized into six major groups: spray-based methods, laser-based direct-write methods, ink dispensing-based methods, tip-based writing methods, and screen printing/dip-coating-based methods [10]-[15]. Among these DW processes, the spray-based methods show the highest technology readiness level [16].

The spray-fabricated sensors reported in the literature are mainly single functional passive type sensors, such as thermocouple, piezoresistive and capacitive sensors [17], [18], which can only passively sense the changes of environmental parameters such as temperature and strain through the responsive changes at the location of the sensors. While piezoelectric transducers are the powerful NDT sensors in various applications, which can work in both active and passive modes, the reports on DW-fabricated piezoelectric transducers are very limited [19]. In the existing reports for active ultrasonic wave excitation, DW serves only as a method to pattern electrodes while the piezoelectric polymer materials are still implemented as separate piezoelectric polymer films formed by traditional material fabrication methods. In such conventional practice, the prior fabricated transducers are subsequently bonded or assembled on the structures to be monitored [5], [17]. Danz reported a piezoelectric stripe sensor manufactured using an air-brush technique. The sensor was used passively for air

[1] Manuscript received on January 26, 2017. This project is supported by the Aerospace Program of A*STAR, Singapore through the project IMRE/12-2P1101, and SERC Grant Number 1121550604.

Z. Shen, S. Chen, L. Zhang, K. Yao, C. Y. Tan are with the Institute of Materials Research and Engineering (IMRE), Agency for Science, Technology and Research (A*STAR), #08-03, 2 Fusionopolis Way, Innovis, Singapore 138634 (+65-64168936; k-yao@imre.a-star.edu.sg).

pressure monitoring [20]. Haque [21] developed a poly(vinylidenefluoride/trifluoroethylene) (P(VDF/TrFE)) ink for inkjet printing and characterized the piezoelectric properties of the printed P(VDF/TrFE) film, while there was no demonstration of inkjet-printed active ultrasonic transducers. It would be a significant technological advancement with great benefits if DW technologies can be effectively applied to produce piezoelectric ultrasonic transducers directly on an aeronautical structure to be monitored.

This paper reports the design, direct-write fabrication, and testing of ultrasonic transducers on a plate structure and a non-destructive testing method for detecting defects using the sensor array comprising the direct-write ultrasonic transducers. The transducers are made of piezoelectric P(VDF-TrFE) polymer coatings that are aerosol-spray deposited and patterned directly on the plate structure to be monitored. The ultrasonic transducers can serve as both the actuators to generate Lamb mode ultrasonic waves and the sensors to detect the waves containing the information about the structural integrity. A short time Fourier transform algorithm and an imaging algorithm are described processing pitch-catch ultrasonic wave spectra to determine the location and the severity of the defects, which is subsequently verified by experimental testing. The implementation of such DW ultrasonic transducers completely eliminates any bonding agent such as glue used to bond the transducers on the structure, thus the mechanical strain coupling between the transducers and the structure can be enhanced. The manual process for individually installing multiple discrete transducers is replaced by the *in situ* batch fabrication of the truly integrated transducers, and thus the consistency and reliability are improved while the global cost over the whole structure is reduced.

II. Design

The structure under monitoring is an aluminum plate with a dimension of 100 mm×100 mm×1.27 mm. Lamb waves can be regarded as a combination of longitudinal waves and vertically polarized shear waves, which are intrinsic ultrasonic wave forms existing in plate structures with parallel free boundaries. Lamb wave-based NDT has drawn great research interest in the last three decades [22]-[27]. For a plate with a thickness *h*, there exist a finite number of propagation Lamb modes at frequency *f*. These modes are specified by their phase velocities. A complete description of the Lamb wave propagation characteristics in plates is normally given in the form of a set of dispersion curves. Each curve represents a specific mode, illustrating the mode's phase velocity as a function of the frequency. The Lamb waves can be divided into two categories: antisymmetric A modes, in which the particle displacement *u* across the thickness is antisymmetric, and symmetric S modes, in which the particle displacement *u* across the thickness of the plate is symmetric. The theoretical expression of the dispersion curves for S modes is [22]:

$$\frac{\tan(qh)}{\tan(ph)} = -\frac{4k^2pq}{(q^2-k^2)^2} \quad (1)$$

and for A modes:

$$\frac{\tan(qh)}{\tan(ph)} = -\frac{(q^2-k^2)^2}{4k^2pq} \quad (2)$$

where $p^2 = \frac{\omega^2}{c_L^2} - k^2$, $q^2 = \frac{\omega^2}{c_T^2} - k^2$, $k = \frac{\omega}{c_p}$; k is the wave number; c_L is the velocity of the longitudinal wave; c_T is the velocity of the transverse wave; c_p is the phase velocity; and ω is the angular frequency of the Lamb wave. The group velocity c_g can be calculated by $\frac{\partial\omega}{\partial k}$. For the 1.27 mm thick aluminum plate, the calculated dispersion curves for both phase velocity and group velocity are shown in Fig. 1.

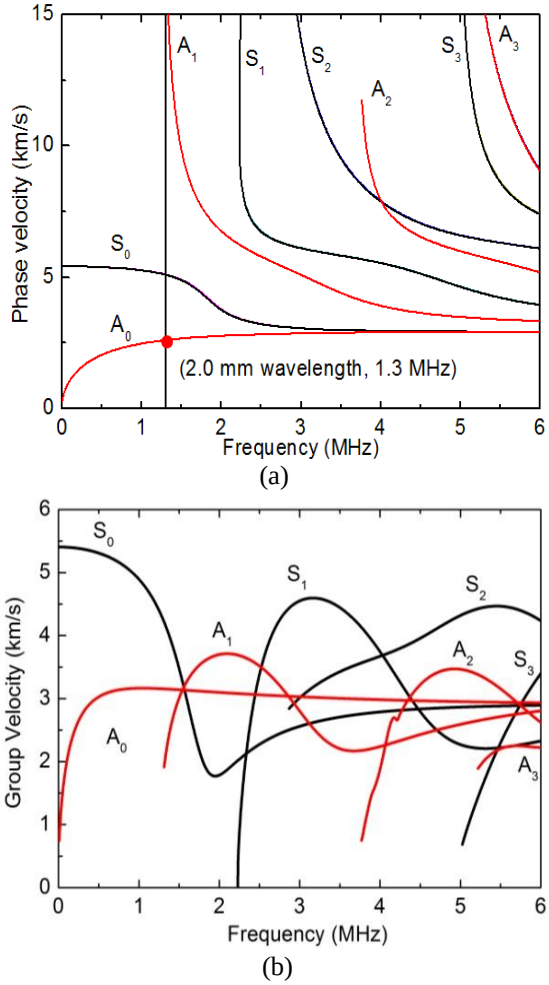

Fig. 1. Dispersion curves for an aluminum plate with the thickness of 1.27- mm (a) phase velocity and (b) group velocity.

The fundamental modes S_0 and A_0 are normally utilized for NDT [23]. Annular array comb electrodes with the period of a wavelength apart are adopted in our design to achieve Lamb mode in the structures (Fig. 2). As reported in [28], 135 degree sectioned annular array comb electrodes can effectively select A_0 mode and can generate omni-directional waves in the plate. The comb electrode causes a relatively high out-of-plane strain and low in-plane strain, which can achieve a stronger coupling to asymmetric Lamb modes than to symmetric Lamb modes [29]. In this work, input signal of 1.3 MHz has been selected to excite the Lamb waves. This is the highest frequency at which only S_0 and A_0 modes exist. The vertical line at 1.3 MHz in Figure 1(a) has two intersections with the A_0 mode and the S_0 mode curves. At 1.3 MHz, only the A_0 and S_0 modes represented by these two intersections can be effectively

excited. From the dispersion curves shown in Fig. 1(a), the A_0 mode has a wavelength of 2.0 mm while the S_0 mode has a wavelength of 3.9 mm at 1.3 MHz. The annular array comb electrodes with a period of 2.0 mm are thus adopted to constructively excite and receive the A_0 mode other than the S_0 mode in the plate (Fig. 2(b)). Four annular array comb electrodes with the spanning angle of 90 degrees are deployed near the four corners of the plate to cover as much detection area as possible. The electrode in each corner is composed of six concentric arcs, with one common electrode trace connecting all the arcs.

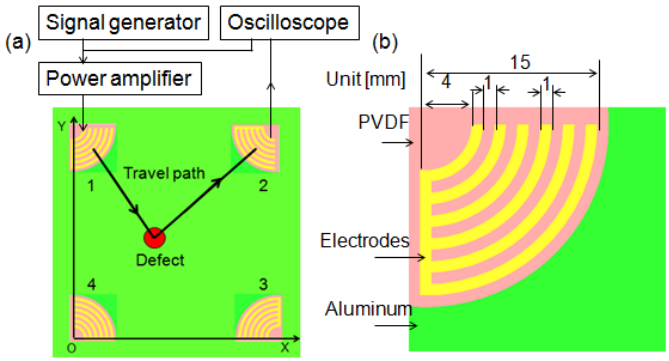

Fig. 2. Schematic illustration of (a) the distribution of the four direct-write ultrasonic transducers on the metal plate, and (b) the dimensions of the annular array comb electrodes.

The DW piezoelectric ultrasonic transducers in this design comprise a piezoelectric film direct-written on the aluminum substrate and the top electrode as described above. When working as an actuator, a voltage applied between the top electrode and the aluminum substrate stresses the piezoelectric film and generates ultrasonic waves in the plate through converse piezoelectric effect. For the transducers used as sensors, electric output is generated in response to the stimulation of passing ultrasonic waves. When the Lamb wave generated by one transducer encounters a defect, the scattered wave would be detected by the other three transducers. Time-of-flight and amplitude of the scattered wave will be analyzed and information such as the location and severity of the defect will be abstracted. The aluminum plate in this design serves as a common ground for all the transducers. In case that the plate under monitoring is nonconductive, for example a composite material, a bottom electrode layer should be DW deposited.

III. Transducers Fabrication and Characterization

P(VDF/TrFE) material was adopted for producing the DW piezoelectric transducers due to its advantages such as light-weight, flexible and superior piezoelectric performance compared to other piezoelectric polymers. P(VDF/TrFE) (72/28 mol%) in the form of pellets was obtained from Solvay, Belgium. The pellets were dissolved in a solvent of mixed dimethylformamide (purity > 99%, Sigma-Aldrich, Singapore) and acetone (purity > 99%, Sigma-Aldrich, Singapore) (1:1 in volume) at a concentration of 5 wt%. The P(VDF/TrFE) films were prepared by aerosol spraying method, which enables low cost and quick coating over a large area with the ability of coating on non-flat surfaces [30], [31]. Before spraying, the surface of the aluminum plate was cleaned with ethanol (purity = 99 %, International Scientific Pte. Ltd. Singapore) and deionized water, and manually polished using sand papers from grade 800 to grade 2400. The aluminum plate was rinsed using deionized water between each polishing. The P(VDF/TrFE) solution was then sprayed on the plate using an air brush (Badger NH200 with M-type nozzle, Badger Air-Brush Co., US) at a pressure of 86.2 kPa. During spray, the P(VDF/TrFE) films were directly patterned with the aid of shadow masks, which were fabricated from stainless steel sheets by laser cutting. The nozzle was moved parallel to the surface at a fixed distance to ensure an even coverage. After the spraying process, the P(VDF/TrFE) films were dried at 100 °C in air for 10 minutes and annealed at 135 °C for 4 hours. The thickness of the films can be controlled from a few micrometers to tens of micrometers by varying the deposition parameters including spraying duration and pressure. P(VDF/TrFE) films with an thickness of about 25 μm (±2 μm) were used in this paper.

The dielectric properties of the P(VDF/TrFE) film were characterized using an impedance analyzer (4294A, Keysight Technologies Inc. US.). The film showed a relative dielectric constant of 13.1 and a dielectric loss (as the ratio of the imaginary part to real part of the permittivity) of 0.03 at 1 kHz at room temperature (Fig. 3(a)), which is comparable to those of spin-coated P(VDF/TrFE) thin films [32], [33]. The polarization-electric field hysteresis loop of the aerosol-sprayed P(VDF/TrFE) film is presented in Fig. 3(b). The film exhibits well saturated ferroelectric hysteresis loop with a remnant polarization of ~70 mC/m^2, which is comparable to that of spin-coated P(VDF/TrFE) films [34].

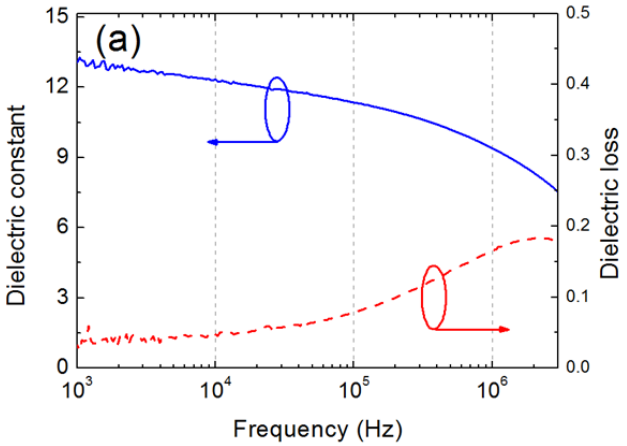

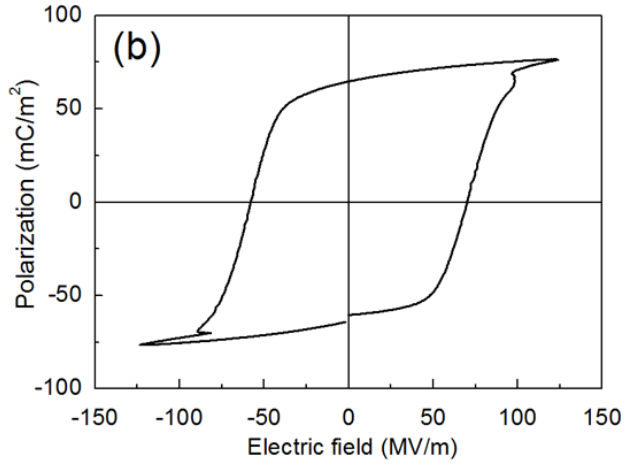

Fig. 3. (a) Frequency dependence of the dielectric constant and dielectric loss of the aerosol-spray coated P(VDF/TrFE) films, and (b) polarization-electric field hysteresis loop of the aerosol-sprayed P(VDF/TrFE) film.

The annular array comb electrodes were deposited by either evaporation or inkjet printing in our experimental demonstration. Here reported was using gold film (200 nm thick) deposited by evaporation with the aid of a shadow mask for direct patterning, which was fabricated from stainless steel sheets by laser cutting. The electrodes were connected to external instrumentation by enameled, 50 μm diameter copper wires (Advent Research Materials, Oxford, UK) which were fixed on the electrodes by conductive epoxy (EC101, Polytec GmbH, Germany). Fig. 4(a) and Fig. 4(b) present photos of the transducer array produced on the- aluminum plate after deposition of patterned P(VDF/TrFE) and gold electrode. The micro-structure of the aerosol-sprayed P(VDF/TrFE) film was examined by a field emission scanning electron microscopy (FESEM, JSM-6700F, JEOL, Japan). The films exhibit smooth and dense morphology (Fig. 4(c)), and thus are appropriate for DW transducer application.

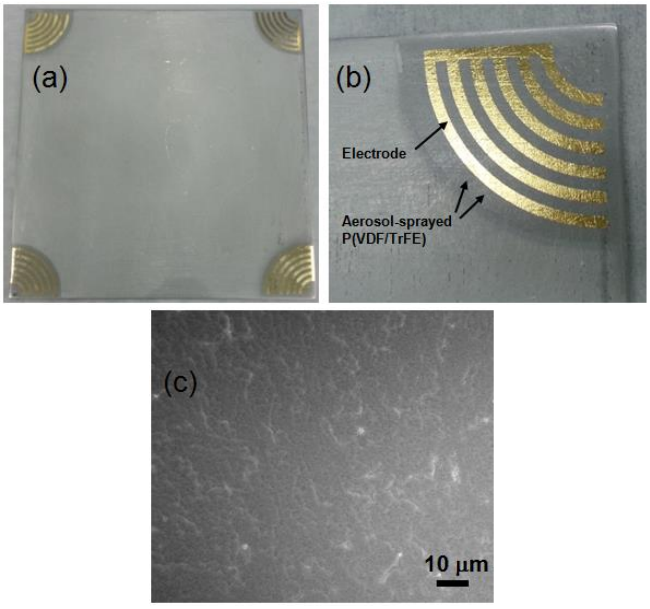

Fig. 4.1 Piezoelectric polymer direct-write transducer array produced on the aluminum plate to be tested. (a) Photo of the whole- aluminum plate with transducers, (b) photo of one transducer at one corner of the- aluminum plate, and (c) FESEM image of the aerosol-spray coated P(VDF/TrFE) films.

The longitudinal piezoelectric coefficient d_{33} [35] of the film after electrical poling was measured using a laser scanning vibrometer (OFV-3001-SF6, PolyTech GmbH) [36]. In the testing, a unipolar 1.5 kHz AC voltage of 30 V amplitude was applied to the sample. The surface of an area covering the regions with and without electrode was scanned (Fig. 5). The effective longitudinal piezoelectric coefficient d_{33} value of the P(VDF/TrFE) thin film is −18 pm/V, under the clamping effect of the substrate. The measured longitudinal piezoelectric coefficient is comparable to the values of spin-coated P(VDF/TrFE) films [32]. When the transducer is excited, both d_{33} and d_{31} effects can induce surface tractions on the plate. The d_{31} effect will induce in-plane traction that tends to trigger the S_0 mode while the d_{33} effect will induce out-of-plane traction that tends to trigger the A_0 mode. The d_{31} coefficient in P(VDF-TrFE) film is only 1/3 to 1/2 of the d_{33} coefficient. Thus, the in-plane piezoelectric strain effect should be smaller than the out-of-plane effect. Because of the smaller in-plane strain effect and the dedicatedly selected electrode period and the input signal frequency, A_0 mode can be more effectively excited than S_0 mode in our experiments.

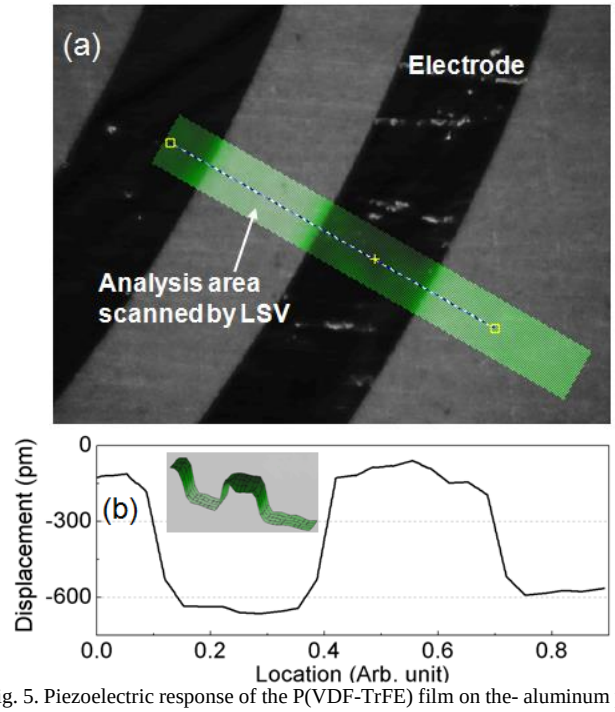

Fig. 5. Piezoelectric response of the P(VDF-TrFE) film on the- aluminum plate measured by a laser scanning vibrometer: (a) Image showing the area characterized by the laser scanning vibrometer. (b) Displacement profile of the instantaneous vibration when the dilatation of the P(VDF/TrFE) film reaches the maximum during the electric driving. The inset shows the three dimensional displacement profile of the area highlighted in (a).

IV. Sensor Testing and Structural Monitoring

For the experimental verification of NDT function with the DW ultrasonic transducers, two experiments were conducted. The first experiment is for detecting the DW -transducers' response to an added copper bar defect with different

thicknesses. The second experiment demonstrates the workability of a DW ultrasonic transducer network for locating the position of an added- aluminum column defect. The added mass simulates the conditions such as icing on the aircraft structure or mass increasing due to corrosion. The schematic of the first experiment is shown in Fig. 6(b) inset. Transducer 1 acting as the actuator was connected with a signal generator (AFG 3000, Tektronix) and Transducer 3 serving as the sensor was connected with an oscilloscope (TDS 3034C, Tektronix). The signal from the generator was also directly connected to the oscilloscope to monitor the input signal. A narrow bandwidth input signal was used to prevent wave dispersion. The input signal was a 13-cycle Hanning windowed tone burst signal with a central frequency of 1.3 MHz and amplitude of 10 V as shown in Fig. 6(a) inset. The received signal by the oscilloscope was recorded as in Fig. 6(a). The received signal after a digital bandpass filtering (passband from 0.9 MHz to 1.7 MHz) shows three packets before 60 μs. The first wave packet is due to the electromagnetic interference [37]. The second wave packet is the Lamb wave directly transmitted from the actuator to the sensor. The third wave packet is due to the Lamb wave reflected from the plate boundary near the actuator. A copper bar with a length of 20 mm and width of 3.0 mm was glued at the center of the aluminum plate as a defect. The longer side of the bar was aligned with the diagonal linking Transducer 2 and Transducer 4. The thickness of the copper bar had the value of 0.5 or 1.0 mm. The 1.0 mm defect was formed by gluing two 0.5 mm thick copper bars together. The bars were glued on the plate using instant adhesive (Loctite 424, UK) and mechanically removed from the aluminum plate after testing. The second wave packet signal reflects the two different defect thicknesses. The packet signals were fast Fourier transformed, and the amplitude of the 1.3 MHz component was shown to decrease as the defect becomes thicker (Fig. 6(b)).

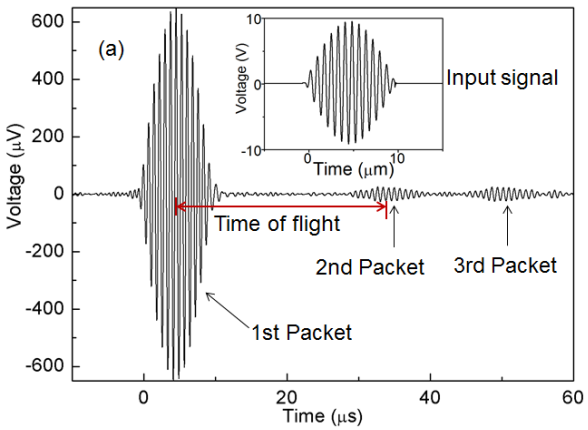

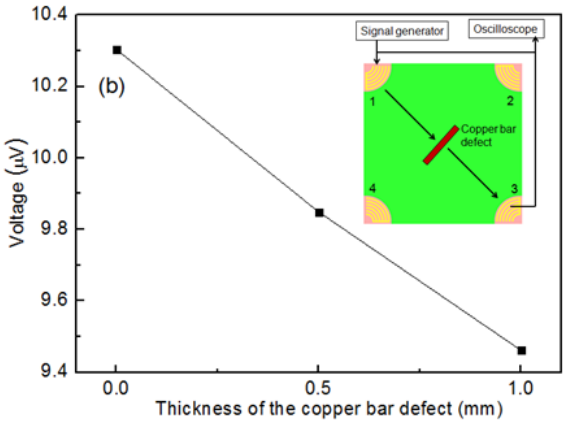

Fig. 6. (a) The received signal by Transducer 3 after bandpass filtering shows three wave packets in the aluminum plate. Transducer 1 serves as the actuator and Transducer 3 serves as the sensor. A copper bar with varied thickness up to 1.0 mm aligned with the diagonal connecting Transducers 2 and 4 was added at the center of the plate as the defect. The inset shows the driving electric signal which is a 13-cycle Hanning windowed tone burst signal with a central frequency of 1.3 MHz. (b) The amplitude of the 1.3 MHz component of the second packet decreases as the defect thickness increases. The inset in (b) shows the experimental setup.

To verify defect locating capabilities of the transducers, an aluminum column with the diameter of 25 mm and the height of 5 mm was glued on the plate as another defect (the experimental setup is shown in Fig. 2(a)). In contrast to the setup in Fig. 6(b) inset, a power amplifier (High-speed Bipolar Power Amplifier 4010, NF Corporation, Japan) was used to amplify the signal from the signal generator with a gain of 100 before it was connected with the actuator. The coordinates of the four transducer electrode annular centers and the defect center are listed in Table I:

TABLE I.
THE COORDINATES OF THE FOUR TRANSDUCERS CENTERS AND THE DEFECT CENTER.

Unit: mm	x-coordinate	y-coordinate
Transducer 1	-0.15	85.49
Transducer 2	80.79	85.08
Transducer 3	80.54	0.00
Transducer 4	0.00	0.00
Defect	55.00	41.00

For locating the defect position, the four transducers were actuated individually. When one transducer served as the actuator, the other three transducers served as the sensors. There are twelve pitch-catch spectra for all the possible transducer pairs. For an intact plate structure before any defect formed on the structure, the twelve spectra were recorded as the reference. After the introduction of the defect the twelve pitch-catch spectra were recorded again. Fig. 7 shows the time domain transmission spectra when Transducer 1 served as the actuator and Transducer 2 served as the sensor. The tone burst signal center was at the 0 s time instance. The spectra show a series of wave packets which are due to the direct transmission of the Lamb wave and its reflection from different boundaries. The wave packet at 20 μs should be the S_0 mode and the subsequent wave packet between 30 μs to 40 μs should be the A_0 mode based on the group velocities of the two modes.

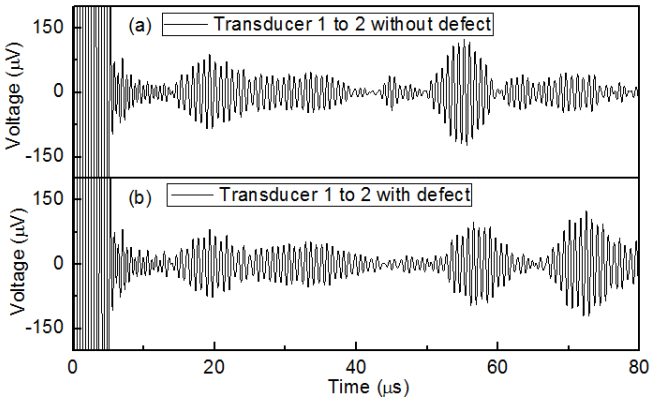

Fig. 7. The time domain transmission spectra from Transducers 1 to 2 with and without defect.

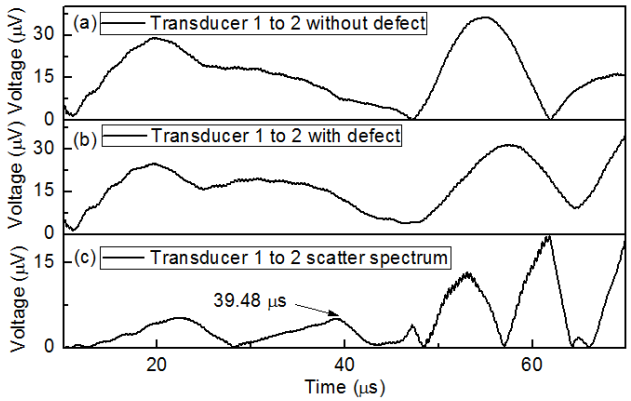

Fig. 8. The short time Fourier transform of the time domain spectra of Transducers 1 and 2 (a) without and (b) with defect; (c) the scatter spectrum by subtracting the spectrum with defect from the spectrum without defect.

A short time Fourier transform (STFT) algorithm was adopted to explore the evolution of the 1.3 MHz component in the transmission spectra as shown in Fig. 7. STFT is a Fourier-related transform used to determine the sinusoidal frequency components in the segments of a longer time domain signal. A rectangular window with the interval of 10 μs is adopted to divide the longer spectra into a series of overlapped short segments. The successive two segments have a fixed time lag of 10 ns, which is determined by the resolution of the oscilloscope used to acquire the data. Each segment is fast Fourier transformed (FFT). The magnitude of the 1.3 MHz component is plotted versus the central time instance in that segment to form the STFT spectra. The reason for the choice of rectangular window interval of 10 μs is because the input tone burst lasts for 10 μs and the received wave packets are supposed to maintain the same time interval.

Fig. 8 (a) and (b) show the STFT spectra of the two time domain spectra in Fig. 7. The scatter spectrum in Fig. 8(c) was obtained by subtracting the STFT spectrum with defect from the one without defect and then taking the absolute value. The scatter spectrum, given by the difference of the unperturbed and the perturbed received signal, reflects the defect induced spectrum change. The starting and ending points of the Lamb wave travel path are regarded to be the origin of the annular array electrodes as listed in Table I. The Lamb wave travel path, scattered by the defect, is 121.93 mm. Based on the second peak on the scatter spectrum whose maximum appears at 39.48 μs as shown in Figure 8(c), the calculated group velocity of A_0 mode is 3.09 km/s, which is close to the theoretical A_0 mode group velocity of 3.15 km/s at 1.3 MHz, as shown in Figure 1(b).

The defect will scatter the Lamb wave packet and result in a maximum on the scatter spectrum. A mapping algorithm reported in [38] and [39] was used to find the location of the defect. In this algorithm, a map representing the aluminum plate was constructed as shown in Fig. 9. For each point on the map, the wave paths from the actuator for exciting the wave to the point and then to the receiver were calculated. The values corresponding to the paths on four scattering spectra (each spectra is based on a pair of transducers located on one side of the square plate) were added. The contrast at each pixel on the map is derived from the sum. The maxima due to the defect scattering from different scatter spectra will sum up and form a maximum on the map. The maxima due to direct transmission and reflection, however, will not have such a constructive effect. The map had the size of 80 mm×80 mm and the pixel size of 1 mm×1 mm. The lower left point of the map is coincided with the origin of the coordinate system shown in Fig. 2(a). The contrast S on each pixel (x, y) was calculated based on (3):

$$S(x,y) = \sum_{i=1}^{4}\sum_{j=1}^{4} f_{ij}^{(s)}\left(\frac{R_r+R_t}{c_g}\right) \quad (3)$$

where $f_{ij}^{(s)}(t)$ denotes the received scattered spectrum by sensor j due to the excitation of actuator i; R_r is the distance between the pixel to transducer j; R_t is the distance between the pixel to sensor i; c_g is the group velocity of the A_0 mode Lamb wave. Scatter spectra of four transducer pairs on the four square plate sides, namely $f_{12}^{(s)}$, $f_{14}^{(s)}$, $f_{23}^{(s)}$, and $f_{34}^{(s)}$, in the time range of 0 to 48 μs, were used in calculating the contrast calculation. Fig. 9 shows the map obtained by (3). It is observed that the location of the maximum magnitude agrees with defect location. This demonstrates the feasibility of the direct-write piezoelectric sensor network for locating defects.

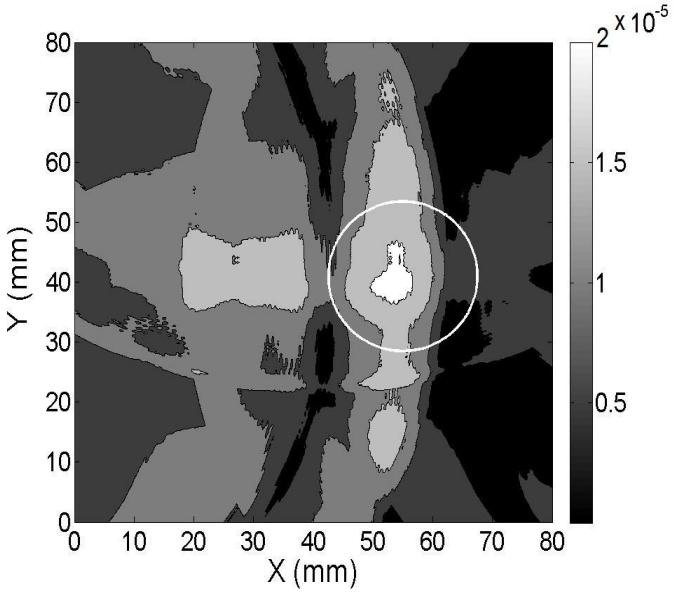

Fig. 9. Digital map synthesized by scattering spectra obtained from the sensor array comprising the 4 direct-write ultrasonic transducers. The magnitude maximum indicates the defect location. The circle shows the true position of the defect.

V. Conclusion

A technology for direct-writing piezoelectric ultrasonic transducers on a plate structure and further monitoring the structural health using the sensor array comprising the multiple direct-write transducers have been developed. The transducers are made of piezoelectric poly(vinylidenefluoride/trifluoroethylene) (P(VDF/TrFE)) polymer coatings that are aerosol-spray deposited and patterned directly on the plate structure to be monitored. The aerosol-spray method can produce high quality dense piezoelectric polymer films with competitive piezoelectric performance properties. Scanning laser vibrometer testing results show that the direct-write P(VDF/TrFE) film has the effective longitudinal piezoelectric coefficient d_{33} value of -18 pm/V with the clamping effect of the substrate. The ultrasonic transducers bearing annular array comb electrodes are designed for generating and selectively detecting fundamental antisymmetric A_0 Lamb mode ultrasonic waves at 1.3 MHz in the plate structure. The ultrasonic transducers can serve as both the actuators to generate ultrasonic waves and the sensors to detect ultrasonic waves. The ultrasonic waves propagating through the plate structure contain the information about the structural integrity. It is demonstrated that four ultrasonic transducers located at the square plate corners forming the transducer array can locate defect on the plate. A short time Fourier transform algorithm and a mapping algorithm by summing up scatter spectra of the multiple transducers are developed for processing signal of the pitch-catch ultrasonic wave spectra to determine the location and the severity of the defects, which is verified by experimental testing results. Further systematic investigations on the potential values of the innovated strategy of using direct-write active ultrasonic transducers for in-situ structural health monitoring in industry applications are demanded.

Acknowledgement

The project team would like to thank Rodrigo Carlana da Silva, Paulo Anchieta da Silva, Sidney Osses Nunes and Tomaz Lazanha from Embraer for the helpful discussions and supports.

References

[1] D. C. Latia, *Nondestructive Testing for Aircraft*. Jeppesen Sanderson, 2002.
[2] W. J. Staszewski and C. Boller, *Health Monitoring of Aerospace Structures-smart Sensor Technologies and Signal Processing*, Wiley, 2004.
[3] Market Report: *Global Non-Destructive Testing (NDT) Equipment Market*, Markets and Markets, 2013.
[4] K. K. B. Hon, L. Li, and I. M. Hutchings, "Direct writing technology-advances and developments," *CIRP Annals-Manufacturing Technology*, vol. 57, pp. 601-620, 2008.
[5] A. Pique and D. B. Chrisey, *Direct-write technologies for rapid prototyping applications: sensors, electronics, and integrated power sources*. Academic Press, 2002.
[6] S. Sampath, H. Herman, and R. J. Greenlaw, *Method and apparatus for fine feature spray deposition*, U.S. Patent No. 6,576,861, 2003.
[7] R. J. Gambino, M. M. Raja, S. Sampath, and R. Greenlaw, "Plasma-sprayed thick film anisotropic magnetoresistive (AMR) sensors," *IEEE Sensors Journal* 4(6), pp. 764-767, 2004.
[8] J. Li, J. P. Longtin, S. Tankiewicz, A. Gouldstone, and S. Sampath, "Interdigital capacitive strain gauges fabricated by direct-write thermal spray and ultrafast laser micromachining," *Sensors and Actuators A: Physical* 133(1), pp. 1-8, 2007. [9] J. Rausch, L. Salun, S. Griesheimer, M. Ibis, and R. Werthschutzky, "Printed resistive strain sensors for monitoring of light-weight structures," *Smart Sensor Phenomena, Technology, Networks, and Systems, Proc. of SPIE 2011*, vol. 7982, pp. 79820H, 2011.
[10] C. Gouldstone, J. Brogan, R. Greenlaw, R. J. Gambino, J. Gutleber, S. Sampath, and J. Longtin, "Embedded resistive strain sensors for harsh environments," *IEEE Aerospace Conference*, pp. 3813-3822, 2006.
[11] W. Nam, J. I. Mitchell, C. Tansarawiput, M. Qi, and X. Xu, "Laser direct writing of silicon field effect transistor sensors," *Applied Physics Letters*, vol. 102, pp. 093504, 2013. [12] R. D. Piner, J. Zhu, F. Xu, S. H. Hong, C. A. Mirkin, ""Dip-pen" nanolithography," *Science*, vol. 283, pp. 661–663, 1999.
[13] W. Y. Chang, T. H. Fang, H. J. Lin, Y. T. Shen, and Y. C. Lin, "A large area flexible array sensors using screen printing technology," *Journal of Display Technology*, vol. *5*(6), pp. 178-183, 2009.
[14] T. Islam, D. Saha, P. M. Hasan, and S. S. Islam, "γ-Al2O3 coated porous silicon for trace moisture detection," *IEEE Sensors Journal*, vol. 11(4), pp. 882-887, 2011.
[15] M. Zirkl, et. al., "An all-printed ferroelectric active matrix sensor network based on only five functional materials forming a touchless control interface," *Adv. Mater.*, vol. 23, pp. 2069-2074, 2011.
[16] L. Zhang, K. Yao, Z. Shen, and C. Y. Tan, "Evaluation of direct-write sensor technology for aeronautical applications," *Technical Report*, Institute of Materials Research and Engineering, Aug. 2013.
[17] B. Thompson and H. S. Yoon, "A self-sensing structure with printed sensors," *Sensors and Smart Structures Technologies for Civil, Mechanical, and Aerospace System 2011, Proc. of SPIE*, vol. 7981, pp. 79814H, 2011.
[18] B. S. Cook, A. Shamim, and M. M. Tentzeris, "Passive low-cost inkjet-printed smart skin sensor for structural health monitoring," *IET Microwaves Antennas & Propagation*, vol. 6, pp. 1536-1541, 2012.
[19] V. T. Rathod, D. R. Mahapatra, A. A. Jeyaseelan, and S. Dutta, "Large-area piezoceramic coating with IDT electrodes for ultrasonic sensing applications," *Smart Sensor Phenomena, Technology, Networks, and Systems Integration 2013, Proc. of SPIE, vol. 8693*, 2013.
[20] R. Danz, B. Elling, A. Buchtemann, and P. Mirow, "Preparation, characterization and sensor properties of ferroelectric and porous fluoropolymers," *Proceedings of 11th International Symposium on Electrets*, 2002, pp. 199-202.
[21] R. I. Haque, R. Vie, M. Germainy, L. Valbin, P. Benaben, and X. Boddaert, "Inkjet printing of high molecular weight PVDF-TrFE for flexible electronics," *Flex. Print. Electron.*, vol. 1, pp. 015001-1-12, 2016.
[22] J. L. Rose, *Ultrasonic Waves in Solid Media*, Cambridge University Press, 1999.

[23] Z. Su, L. Ye, and Y. Lu, "Guided Lamb waves for identification of damage in composite structures: a review," *Journal of Sound and Vibration*, vol. 195, pp. 753-780, 2006.

[24] X. Zhao, H. Gao, G. Zhang, B. Ayhan, F. Yan, C. Kwan, and J. L. Rose, "Active health monitoring of an aircraft wing with embedded piezoelectricsensor/actuator network: I. Defect detection, localization and growth monitoring," *Smart Mater. Struct.*, vol. 16, pp. 1208-1217, 2007.

[25] R. S. C. Monkhouse, P. D. Wilcox, and P. Cawley, "Flexible interdigital PVDF transducers for the generation of Lamb waves in structures," *Ultrasonics*, vol. 35, pp. 4890498, 1997.

[26] A. Raghavan and C. E. S. Cesnik, "Review of guided-wave structural health monitoring," *The Shock and Vibration Digest*, vol. 39, pp. 91-114, 2007.

[27] M. Manka, M. Rosiek, A. Martowicz, T. Stepinski, and T. Uhl, "Lamb wave transducers made of piezoelectric macro-fiber composite," *Struct. Control Health Monit.*, vol 20, pp. 1138-1158, 2012.

[28] H. Gao, M. J. Guers, and J. L. Rose, "Flexible ultrasonic guided wave sensor development for structural health monitoring," *Proc. of SPIE*, vol. 6176, pp. 61761-l-12, 2006.

[29] J. P. Koduru and J. L. Rose, "Transducer arrays for omnidirectional guided wave mode control in plate like structures," *Smart Mater. Struct.*, vol. 22, pp. 1-10, 2013.

[30] C. Girotto, B. P. Rand, J. Genoe, and P. Heremans, "Exploring spray coating as a deposition technique for the fabrication of solution-processed solar cells," *Solar Energy Materials & Solar Cells*, vol. 93, pp. 454–458, 2009.

[31] S. Na, B. Yu, S. Kim, D. Vak, T. Kim, J. Yeo, and D. Kim, "Fully spray-coated ITO-free organic solar cells for low-cost power generation," S*olar Energy Materials & Solar Cells*, vol. 94, pp. 1333–1337, 2010.

[32] S. Chen, K. Yao, E. H. F. Tay, and L. S. L. Chew, "Comparative investigation of the structure and properties of ferroelectric poly(vinylidene fluoride) and poly(vinylidene fluoride–trifluoroethylene) thin films crystallized on substrates," *Journal of Applied Polymer Science*, vol. 116, pp. 3331, 2010.

[33] X. He and K. Yao, "Crystallization mechanism and piezoelectric properties of solution-derived ferroelectric poly(vinylidene fluoride) thin films," *Applied Physics Letters*, vol. 89, pp. 112909-1-3, 2006.

[34] S. Chen, K. Yao, E. H. F. Tay, C. L. Liow, "Ferroelectric poly(vinylidene fuoride) thin films on Si substrate with the β-phase promoted by hydrated magnesium nitrate," *Journal of Applied Physics*, vol. 102, pp. 104108, 2007.

[35] H. S. Nalwa, *Ferroelectric Polymers: Chemistry: Physics, and Applications*. New York, Marcel Dekker Inc. 1995, pp. 859.

[36] K. Yao and F. E. H. Tay, "Measurement of longitudinal piezoelectric coefficient of thin films by a laser scanning vibrometer," *IEEE Transactions on Ultrasonics, Ferroelectrics, and Frequency Control*, vol. 50, pp. 113-116 and front cover page, 2003.

[37] P. D. Wilcox, *Lamb wave inspection of large structures using permanently attached transducers*, Ph.D. Thesis, University of London, 1998.

[38] C. H. Wang, J. T. Rose, and F-K Chang, "A synthetic time-reversal imaging method for structural health monitoring," *Smart Mater. Struct.*, vol. 13, pp. 415–423, 2004.

[39] Y. Lu, L. Ye, and Z. Su, "Crack identification in aluminium plates using Lamb wave signals of a PZT sensor network," *Smart Mater. Struct.*, vol. 15, pp. 839-849, 2006.